Journal of Chromatography A, 1216 (2009) 5365–5376

Contents lists available at ScienceDirect

Journal of Chromatography A

journal homepage: www.elsevier.com/locate/chroma

Identification of uranyl binding proteins from human kidney-2 cell extracts by immobilized uranyl affinity chromatography and mass spectrometry

Alain Dedieu, Frédéric Bérenguer, Christian Basset, Odette Prat, Eric Quéméneur, Olivier Pible, Claude Vidaud*

CEA/IBEB/SBTN, F-30207 Bagnols sur Cèze, France

ARTICLE INFO

Article history:
Received 16 March 2009
Received in revised form 6 May 2009
Accepted 11 May 2009
Available online 18 May 2009

Keywords:
IMAC
Protein–metal interactions
Uranium
Proteomics
Metal-docking prediction algorithm
Aminophosphonate groups

ABSTRACT

To improve our knowledge on protein targets of uranyl ion (UO_2^{2+}), we set up a proteomic strategy based on immobilized metal-affinity chromatography (IMAC). The successful enrichment of UO_2^{2+}-interacting proteins from human kidney-2 (HK-2) soluble cell extracts was obtained using an ion-exchange chromatography followed by a dedicated IMAC process previously described and designed for the uranyl ion. By mass spectrometry analysis we identified 64 proteins displaying varied functions. The use of a computational screening algorithm along with the particular ligand-based properties of the UO_2^{2+} ion allowed the analysis and categorization of the protein collection. This profitable approach demonstrated that most of these proteins fulfill criteria which could rationalize their binding to the UO_2^{2+}-loaded phase. The obtained results enable us to focus on some targets for more in-depth studies and open new insights on its toxicity mechanisms at molecular level.

1. Introduction

The screening of protein targets for toxic metals such as uranium remains a difficult challenge when a few have to be distinguished from thousands of proteins in biological extracts. There is extensive literature related to its adverse effects which are observed in different organs [1–3] and particularly in the kidneys where the renal proximal tubules are damaged by uranium salts [4–8]. Uranium in solution is mainly found under the form of hexavalent uranyl cation UO_2^{2+} and its toxicity might result from the ability to bind strongly to biomolecules, forming complexes with both nucleotides [9–11] and proteins [12–16]. Transcriptomic and proteomic studies highlighted gene modulation and protein expression when such cells were grown in uranyl-containing medium [17–19]. Nevertheless, intracellular vehicles of this ion are still largely unknown leading to an ill-documented toxicodynamics at the molecular level.

Selective capture of UO_2^{2+}-binding proteins from small bio-fluid samples such as cell lysates needs a selective and low-consumption separation strategy. An initial two-dimensional chromatography approach led to some target identification in blood samples [13] but the process required quantities of samples too large to be easily applied to cell extracts. An *in silico* screening method was developed for uranyl docking prediction in proteins [20]. Recently, it led to successful experimental validation of a proposed protein target for the uranyl cation, identified through screening structures from the Protein DataBank (submitted). This powerful strategy depends on the availability of structural information for a given protein to investigate direct interaction with UO_2^{2+}. Immobilized metal-affinity chromatography (IMAC) is now a widely accepted technique for the separation of protein targets of metals. Classic chelating groups such as iminodiacetic acid (IDA) or nitrilo-tri-acetic acid (NTA) are currently used to complex metal ions such as Co^{2+} or Ni^{2+} for the capture of His-tagged proteins. The use of other divalent or trivalent cations has also been reported for designing metal-affinity based separations [21–24], particularly for phospho-proteome analysis [25–29], biomarker identification [21,30], profiling [31,32] or surface topography studies [33–35].

However, these chelating groups are inappropriate for uranyl chelation [36]. UO_2^{2+} is classified as a hard Lewis cation and effective chelating agents for uranyl are thus expected to contain hard Lewis bases, such as carboxylate, phenolate or phosphonate functional groups. Duolite C467™ beads contain aminophosphonic groups and could therefore be considered for the effective sorption of UO_2^{2+} ions. A dedicated uranyl-loaded phase was first designed and previously validated [15].

Here we report on the application of this validated IMAC system for the enrichment and identification of uranyl binding proteins of the human kidney-2 (HK-2) cell extract. We set up first a prefractionation of the soluble protein extract leading to four fractions, in which the abundant proteins were identified by two-dimensional

* Corresponding author. Tel.: +330 4 66 79 67 62; fax: +330 4 66 79 19 05.
E-mail address: claude.vidaud@cea.fr (C. Vidaud).

0021-9673/$ – see front matter © 2009 Elsevier B.V. All rights reserved.
doi:10.1016/j.chroma.2009.05.023

polyacrylamide gel electrophoresis (2D-PAGE) and mass spectrometry. The fractions were then subjected to the IMAC system, from which 64 different proteins were isolated and identified. This process was well adapted to small amount of proteins, and the experimental conditions (pH, ionic strength, carbonate supplementation) were close to physiological conditions favoring thus the selection of proteins able to bind uranyl ions *in vivo*. Wondering about the specificity of this enrichment, we used a complementary approach and demonstrated that the enriched populations from Fe or UO_2-IMAC were significantly different. Then, the collection of UO_2^{2+} binding proteins was analyzed and their metal binding properties are discussed opening new insights on the uranyl toxicity.

2. Experimental

All experiments were conducted at room temperature unless otherwise stated.

2.1. Materials

Main reagents and salts were from Sigma–Aldrich Fluka (Saint Quentin Fallavier, France). Duolite C467™ was provided by Rohm & Haas (Philadelphia, PA, USA) and initially used in its sodium salt form. Natural uranium was provided by CEA and used as uranyl acetate in 0.1 M aqueous solution, pH ∼4. Spectrapor membranes (6000–8000) were used for the dialysis. Ultra-pure water (18 MΩ) was provided by a Milli-Q (Millipore, Billerica, MA, USA) installation.

The quantity of uranyl species in the solutions was determined by UV–vis spectroscopy (Cary 50, Varian, Palo Alto, CA, USA), or ICP-MS (PQ Excell Option S, Thermoptek, Vienna, Austria), depending on the uranium concentration range. Purified proteins for biochemical assays were from Sigma.

2.2. HK-2 cell culture

HK-2 cells were grown in a 500 cm^2 Triple Flask (Nalge Nunc International, Roskilde, Denmark) in D-MEM/F-12 medium (Gibco, Invitrogen, Cergy Pontoise, France) supplemented with penicillin (50 μg/mL) and streptomycin (50 μL/mL) from Gibco Invitrogen and 10% fetal bovine serum (HyClone, Logan, UT, USA). Cells were incubated at 37 °C in 5% CO_2. When necessary, the cells were washed with 0.15 M NaCl, 0.05 M sodium phosphate pH 7.4 buffer after medium elimination, trypsin treated (Gibco Invitrogen), and then harvested by centrifugation. Cell pellets (∼10^8 cells) were stored at −80 °C.

2.3. Soluble protein extraction

Frozen cell pellets were thawed on ice and resuspended with 1 mL of 0.05 M *N*-2-(hydroxyethyl)piperazine-*N*′-(2-ethanesulfonic acid) (HEPES) buffer pH 8 for 20×10^6 cells. An EDTA-free protease inhibitor cocktail (Roche, Mannheim, Germany) was added according to the manufacturer instructions and the cells were broken at 1000 bars by disruption (Constant Cell Disruptor System, Constant System Ltd., UK). DNA was eliminated through two successive spermin (Sigma), precipitations at 4 °C, followed by incubation for 1 h 30 min at 4 °C with gentle stirring and final ultracentrifugation (1 h at 4 °C and 100,000 × *g*). The final supernatant was then dialysed overnight against 0.02 M HEPES buffer pH 8.0. A slight precipitate was eliminated by centrifugation (10 min, 4 °C and 3000 × *g*). The protein content was measured by checking the $A_{260/280\,nm}$ ratio and controlled by bicinchoninic acid (BCA) assay (Interchim, Montluçon, France).

2.4. Ion-exchange

The chromatography was monitored by a Åkta Purifier 10 System (GE Healthcare, Uppsala, Sweden). Samples of the extract (5 mL) were injected into a 5 mL HiTrap DEAE FF (GE Healthcare) column. The process was highly reproducible, allowing the collection of four different populations. Binding occurred in 0.02 M HEPES pH 8.0 buffer at 0.5 mL/min leading to the flow-through (P1). Then a linear gradient until 0.5 M NaCl led to the collection of three other populations (P2–P4). No protein output was observed between 0.5 and 1 M NaCl. For each collected population, the $A_{260/280\,nm}$ and protein content (BCA assay) were checked before dialysis and concentration for further use.

2.5. Proteomic analysis of the populations (P1–P4)

To identify the major proteins of each previously collected population a proteomic analysis was performed. 2D-PAGE and in-gel digestion have been described elsewhere [13]. The gels were digitized at 300 dpi using a UMAX scanner (GE Healthcare) and finally analyzed using Image Master 2D Platinium software (GeneBio, Geneva, Switzerland).

2.6. Preparation of protein samples for IMAC

Protein samples were extensively dialysed overnight against 50 mM HEPES, 500 mM NaCl and 0.05% Brij, pH 7.4, as binding buffer. The protein concentration was adjusted to the selected $A_{279\,nm}$. A few micro-liters of concentrated $NaHCO_3$ solution were added to reach 1 mM as final concentration.

2.6.1. Support preparation for IMAC

A stock of 2.5 g of Duolite C467 beads was prepared as previously described [15]. Stock beads were loaded either with uranyl [15] or ferric ions as follows, and stored at 4 °C for further use and controls.

2.6.2. Immobilized ferric support preparation for IMAC

Ferric chloride was also used as loaded metal to control metal binding selectivity. The process for ferric loading onto the support was strictly identical to uranyl [15]. Briefly, stock beads (0.25 mL) were added to 1 mL of 50 mM acetate pH 4 buffer. Then ferric chloride (0.1 M) in 50 mM acetate pH 4 buffer was contacted with the beads with overnight agitation at room temperature, while respecting a final concentration of 0.05 M. The supernatant was removed and stored for controls. The loaded support was then washed eight times by 3 mL for 10 min and dialysed twice for 90 min with the acetate buffer. The beads were then conditioned at pH 7.4. All the washing steps were followed by spectrophotometry to control the stability of the binding. The distribution coefficient was not determined in the case of ferric loaded support, but we controlled that metal desorption was very low. Metal free and metal loaded beads were dialysed twice for 90 min and overnight against 250 mL of 50 mM HEPES, 0.5 M NaCl pH 7.4. Before any protein chromatography, 0.05 mL of this support was rinsed six times using the same 50 mM HEPES, 0.5 M NaCl pH 7.4 buffer plus 0.05% Brij as surfactant.

2.6.3. Protein capture by IMAC

Batch systems were chosen according to the sample size. Two biological replicates were processed for each population from the ion-exchange. Briefly, two aliquots of 1 mL of a previously prepared protein solution were adjusted to 0.2 ± 0.02 $A_{279\,nm}$ (∼0.15–0.17 mg/mL in BCA assay) and brought into contact in parallel with 50 μL of uranyl-bound or free beads (room temperature, gentle stirring) for 60 min. Protein binding was monitored by UV measurements in the supernatants. The supernatants were dis-

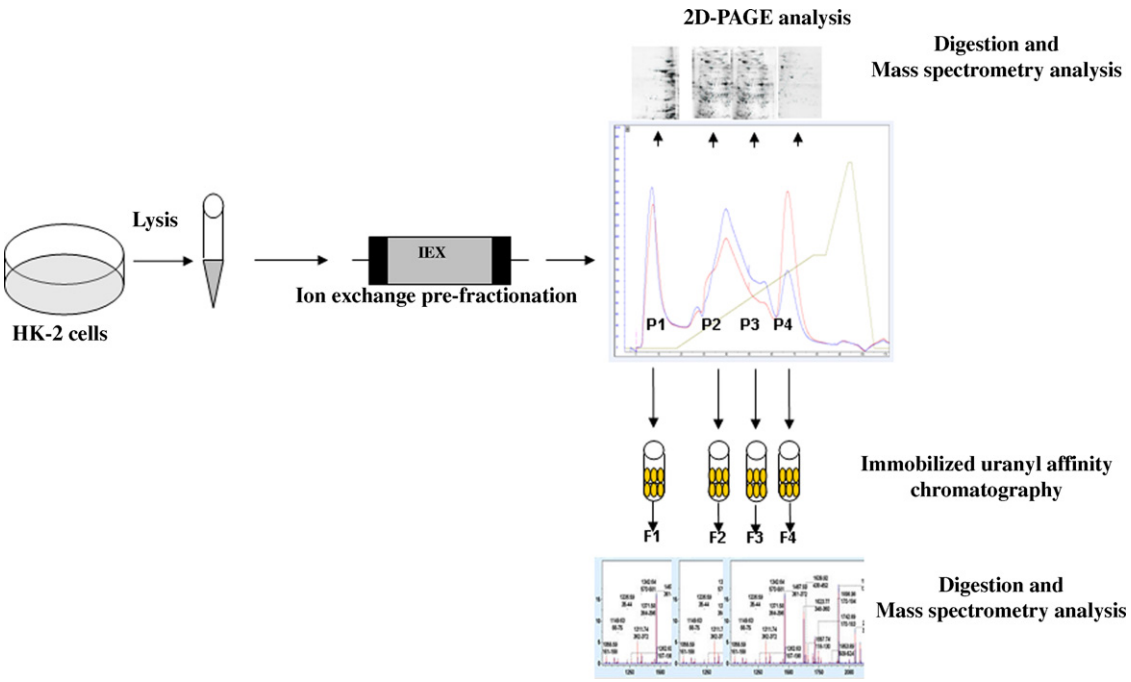

Fig. 1. Schematic representation of the IMAC process. HK-2 lysates were first pre-fractionated into P1–P4 populations by ion-exchange chromatography. The absorbances $A_{260\,nm}$ (red trace) and $A_{280\,nm}$ (blue trace) were monitored during the process and the populations eluted in an NaCl gradient (green trace). These populations were checked by 2D-PAGE and mass spectrometry analysis before being submitted to the IMAC process. F1–F4 captured and eluted fractions were analyzed for protein identification by mass spectrometry. (For interpretation of the references to color in this figure legend, the reader is referred to the web version of the article.)

carded and the beads washed seven times with 1 mL of the binding buffer and dialysed overnight against the same buffer. Again the supernatants were discarded. The proteins were eluted by bringing the metal free and metal loaded supports into contact with either a 0.2 M sodium carbonate solution for uranyl-loaded beads, or 0.2 M citrate pH 7.4 buffer for ferric loaded beads, and for 60 min. The eluates were collected, desalted in ammonium carbonate by multiple concentration-dilution steps in micro-concentrator systems for further protein identification.

2.7. Identification of the captured proteins

2.7.1. Digestion of the affinity purified aliquots

Desalted solutions were buffered with 100 mM ammonium hydrogencarbonate and denatured by adding urea (1 M final concentration). Cysteine reduction/ carbamidomethylation were carried out for 15 min in 1 mM DTT at 60 °C, and for 15 min at room temperature in 3.75 mM of iodoacetamide (final concentration). Digestion was achieved with porcine trypsin (Roche) at an *E*/*S* ratio 1/50 of 14–18 h at 37 °C, and then stopped by adding trifluoro acetic acid (TFA) to a final concentration of 0.1%.

2.7.2. Nano-liquid chromatography on-line with electrospray ionisation tandem mass spectrometry (nano-LC–ESI-MS/MS)

Two independent analysis were performed for each sample. Nano-liquid chromatography (Nano-LC) separations were performed on an UltiMate 2D-NanoLC system. The nano-LC device was coupled to the Bruker Esquire 3000 plus ion trap (nano-ESI source). The complete LC–MS setup was controlled by the HyStar software.

Water/acetonitrile/formic acid (95/5/0.1, v/v/v) was used as solvent A and water/acetonitrile/formic acid (20/80/0.1, v/v/v) as solvent B. 15 μL of the sample diluted in solvent A were injected at a flow rate of 30 μL/min and trapped on an LC Packings precolumn (300 μm id × 5 mm C18-PepMAP 100). Separations were performed on a nanoscale C18 LC Packings column (75 μm id × 15 cm C18-PM), using a 30 min linear gradient (0–50%) at a flow rate of 200 nL/min. Mass spectrometry was performed on-line using the ion trap in positive mode and data-dependent MS to MS/MS switch regime (ICC target: 30,000 – Scan range 100–2000 *m*/*z*, target mass 750 *m*/*z*). The complete LC–MS setup was controlled by HyStar software.

2.7.3. Proteomic data analysis

From the MS/MS analysis, the proteins were identified using non-deconvoluted spectra on a local MASCOT server (2.2.1; Matrix Science, London UK). Peptide tolerance was set at ±0.3 Da. The maximum number of miscleavages was set at one, cysteine carbamidomethylation (C) set as a fixed modification and methionine oxidation (M) as a variable modification. Proteins were identified with two sequenced peptides and a statistical score above identity for each peptide (as defined by MASCOT).

2.8. Ingenuity analysis

Ingenuity Pathways Analysis (IPA 6.0) software (Ingenuity Systems, Mountain View, CA, USA) uses the Ingenuity Pathways Knowledge Base (IPKB), a curated database of biological networks consisting of millions of individually modelled peer-reviewed pathway relationships. A more detailed description of this database and IPA 6.0 software can be found on the website (http://www.ingenuity.com). This computational tool was used for protein annotations, to detect protein–protein interactions, potential functions or pathways, and highlight possible regulatory networks. Protein networks were algorithmically generated for each fraction of chromatography. In such a network, proteins or genes are represented as nodes, and the protein–protein interactions are represented as lines between two nodes. All edges are supported by at least one reference from the literature and displayed with various labels. The proteins or genes from our data set were annotated with biological functions or diseases, and a Fisher's exact test was used to validate a *p*-value determining the probability that each biological function assigned to that data set is due to chance alone.

Table 1
Proteomic analyses of the four populations (P1–P4) from the ion-exchange pre-fractionation.

Gel	Protein name	Swiss Prot accession number	Spot number	Mascot score
P1	Alpha-enolase	P06733	1 – 2 – 3 – 4 – 5	40 – 82 – 99 – 72 – 89
	Transketolase	P29401	6 – 7 – 8 – 37	72 – 92 – 80 – 543
	Superoxide dismutase [Mn]	P04179	9	54
	Glucose-6-phosphate isomerase	P06744	10	98
	Phosphoglycerate kinase 1	P00558	11 – 12 – 13	99 – 55 – 63
	Annexin A1	P04083	14	111
	Annexin A2	P07355	15 – 16	113 – 72
	Fructose-bisphosphate aldolase A	P04075	17	124
	Malate dehydrogenase	P40926	18	73
	Short chain 3-hydroxyacyl-CoA dehydrogenase	Q16836	19	88
	Ras suppressor protein 1	Q15404	20	90
	Carbonic anhydrase 2	P00918	21	88
	Protein DJ-1	Q99497	22 – 23	69 – 57
	Phosphatidylethanolamine-binding protein	P30086	25	116
	Peptidyl-prolyl cis-trans isomerase A	P62937	26 – 27	87 – 111
	Nucleoside diphosphate kinase B	P22392	28	93
	Cofilin-1	P23528	29	62
	Profilin-1	P07737	30 – 31	70 – 96
	FK506-binding protein 1A	P62942	32	70
	Profilin-2	P07737	33	61
	Calgizzarin	P31949	34	56
	10 kDa heat shock protein, mitochondrial	P61604	34	88
	Macrophage migration inhibitory factor	P14174	35 – 36	174 – 160
	Ubiquitin	P62988	38	76
P2	Elongation factor 2	P13639	1	203
	Vinculin	P18206	2	1237
	Ezrin	P15311	3	567
	Radixin	P35241	4	167
	78 kDa glucose-regulated protein	P11021	5	451
	Heat shock cognate 71 kDa protein	P11142	6	157
	Heat shock 70 kDa protein	P08107	7	337
	Protein disulfide-isomerase A3	P30101	10 – 11	69 – 53
	WD-repeat protein 1	O75083	8 – 9	41 – 41
	Alcohol dehydrogenase	P14550	12 – 13 – 14 – 15 – 16 – 17 – 32 – 33 – 35	645 – 88 – 72 – 39 – 49 – 41 – 46 – 72 – 41
	M-phase phosphoprotein 8	Q99549	13	43
	Aldose reductase	P15121	13 – 14	438 – 391
	Annexin A2	P07355	15	245
	L-lactate dehydrogenase A chain	P00338	36 – 17	178 – 125
	Phosphoglycerate mutase 1	P18669	15 – 31 – 33 – 34 – 32 – 35 – 40	55 – 65 – 279 – 55 – 55 – 86 – 54
	Annexin A5	P08759	22	413
	Chloride intracellular channel proteine 1	O00299	23	203
	Rho GDP-dissociation inhibitor 1	P52565	36	37
	Annexin A5	P08758	24 – 50	45 – 64
	Lactoylglutathione lyase	Q04760	48	61
	Cathepsine D	P07339	49	108
	Chloride intracellular channel proteine 4	Q9Y696	49	155
	Glutathione S-transferase P	P09211	50 – 18	137 – 215
	Transaldolase	P37837	19	267
	L-lactate dehydrogenase B chain	P07195	19 – 20 – 21	712 – 74 – 57
	Nicotinate-nucleotide pyrophosphorylase	Q15274	21 – 25	52 – 34
	Annexin A4	P09525	26 – 28	733 – 55
	Glutathione transferase omega-1	P78417	27	50
	NG,NG-dimethylarginine dimethylaminohydrolase 2	O95865	28	94
	Glucosamine-6-phosphate isomerase	P46926	29	260
	GBLP_HUMAN	P63244	30	535
	Vacuolar ATP synthase subunit E	P36543	30	99
	Oligoribonuclease	Q9Y3B8	37	51
	Zinc finger protein 646	O15015	37	442
	6-phosphogluconolactonase	O95336	38	111
	Endoplasmic reticulum protein	P30040	38 – 53	296 – 38
	Heat-shock protein beta-1	P04792	53	48
	Ribosyldihydronicotinamide dehydrogenase	P16083	52	47
	Peroxiredoxin-6	P30041	52 – 37	380 – 296
	ETHE1 protein	O95571	39	64
	Triosephosphate isomerase	P60174	39 – 42	292 – 102
	Hypoxanthine-guanine phosphoribosyltransferase	P00492	40	110
	Cardiotrophin-like cytokine factor 1	Q9UBD9	41	35
	Dihydropteridine reductase	P09417	41	138

Table 1(*Continued*)

Gel	Protein name	Swiss Prot accession number	Spot number	Mascot score
	Thioredoxin-dependent peroxide reductase	P30048	51	1481
	Glutathione S-transferase P	P09211	51 – 37 – 29 – 30	473 – 253 – 88 – 195
	Peroxiredoxin-1	Q06830	43 – 47	331 – 189
	Superoxide dismutase [Mn]	P04179	44	54
	Heterogeneous nuclear ribonucleoprotein A1	P09651	45 – 30	189 – 52
	Heterogeneous nuclear ribonucleoprotein	P22626	46 – 30	54 – 40
	Small ubiquitin-related modifier 2	P61956	54	72
	Nucleoside diphosphate kinase A	P15531	55	92
	Rho GDP-dissociation inhibitor 1	P52565	64	731
	Protein CutA	O60888	56	29
	Coactosin-like protein	Q14019	57	758
	Superoxyde dismutase [Cu–Zn]	P00441	58	254
	Thioredoxin	P10599	59	349
	Coactosin-like protein	Q14019	60	20
	Ubiquitin-conjugating enzyme E2	P61088	61	188
	Uncharacterized protein C6orf115	Q9P1F3	62	48
	Protein S100-A11	P31949	63	167
P3	Elongation factor 2	P13639	1	92
	Heat shock protein	P07900	2	74
	Protein disulfide-isomerase A4	P13667	3	60
	Heat shock cognate 71 kDa protein	P11142	4	145
	Heat shock 70 kDa protein 1	P08107	5	83
	WD-repeat protein 1	O75083	6	89
	Neutral alpha-glucosidase AB	Q14697	7	68
	ERO1-like protein alpha	Q96HE7	8	82
	Calreticulin	P27797	9	372
	Protein disulfide-isomerase	P07237	10	843
	Histone binding protein RBBP	Q09028	11	64
	Prolyl 4-hydroxylase subunit alpha-1	P13674	12	234
	Adenylyl cyclase associated protein 1	Q01518	13 – 14	120 – 20
	Gamma-enolase	P09104	15	109
	Elongation factor 1-gamma	P26641	16	82
	40S ribosomal protein SA	P08865	17	65
	Actin B	P60709	18 – 19 – 22 – 23 – 26	74 – 235 – 143 – 54 – 56
	Actin A	P62736	34 – 18 – 22	70 – 80 – 114
	Adenosylhomocysteinase	P23526	20	74
	Thioredoxin-like protein 2	O76003	21	74
	Complement component 1	Q07021	24	65
	Nicotinate-nucleotide pyrophosphorylase	Q15274	24	48
	Spermidine synthase	P19623	25	70
	40S ribosomal protein SA (P40)	P08865	26	135
	Proteasome activor complex subumit 3	P61286	27	124
	Proteasome subunit alpha type 1	P25786	28 – 38	72 – 90
	Proteasome subumit alpha type 4	P25789	33 – 34 – 35	290 – 35 – 69
	Proteasome subumit alpha type 3	P25788	32	203
	14-3-3 protein zeta/delta	P63104	32	63
	Proteasome subunit beta type 3	P49720	36	54
	Proteasome subunit alpha type 6	P60900	37	96
	Proteasome subumit beta type 6	P28072	40	46
	U6SnRNA-associated Sm-like	P62310	41	41
	Eukaryotic translation initiation factor 5A	P63241	42	59
P4	Adenylate kinase isoenzyme 5	Q9Y6K8	1	55
	Glucosidase 2 beta subunit	P14314	2	57
	Heat shock protein HSP 90-alpha	P07900	3 – 4	126 – 138
	78 kDa glucose-regulated protein	P11021	5	188
	Heat shock cognate 71 kDa protein	P11142	6	77
	Protein disulfide-isomerase	P07237	7	150
	Calreticulin	P27797	8	84
	Stress-70 protein	P38646	9	59
	Protein disulfide-isomerase A3	P30101	10	62
	Protein SET	Q01105	11 – 17	61 – 60
	Spermine synthase	P52788	12	76
	Actin, cytoplasmic 1	P60709	13	80
	Actin, cytoplasmic 1	P60709	14	56
	Macrophage migration inhibitory factor	P14174	15	70
	Elongation factor 1-gamma	P26641	16	70
	Glucosidase 2 beta subunit	P14314	18	155
	L-lactate dehydrogenase B chain	P07195	19	56
	Complement component 1	Q07021	20	61
	Acidic leucine-rich nuclear phosphoprotein 32 A	P39687	21	58

Table 1(*Continued*)

Gel	Protein name	Swiss Prot accession number	Spot number	Mascot score
	Acidic leucine-rich nuclear phosphoprotein 32 B	Q92688	22	54
	14-3-3 protein zeta/delta	P63104	23	102
	14-3-3 protein beta/alpha	P31946	24	63
	Chloride intracellular channel protein 1	O00299	25	76
	GTP-binding nuclear protein Ran (GTPase Ran)	P62826	26 – 28	59 – 58
	Ubiquitin carboxyl-terminal hydrolase isozyme L1	P09936	27	58
	Proteasome subunit alpha type 6	P60900	29	58
	Calmodulin	P62158	30	59

After 2D-PAGE separations, the proteins were identified by peptide fragmentation by Nano-LC–ESI-MS/MS. Their identifications were established with two sequenced peptides and a statistical score above identity.

2.9. In silico analysis

UniProtKB/Swiss Prot Release 55 was used to screen the proteins selected after IMAC enrichment to PDB entries. Our computational screening algorithm was then applied to each PDB entry as previously published [20]. A theoretical "score" of less than −500 is considered to be significant since it lies inside the mean ± 1 SD range of distribution of the UO_2^{2+} specific binding site (paper under submission). This score likens to potential energy of the protein–metal complex; thus the more negative value relates to the more favorable energy.

3. Results and discussion

HK-2 cells are considered to be representative of human kidney proximal tubule cells, a target organ of uranyl [37]. To isolate uranyl binding proteins from small biological samples, we needed an efficient IMAC technique, such as our validated uranyl-loaded Duolite C467^{TM} support [15]. A diagram of the process is shown in Fig. 1.

3.1. Pre-fractionation of the cell extracts

The cells were lyzed in the presence of protease inhibitors. We performed a pre-fractionation of this crude extract by ion-exchange chromatography to facilitate the identification and capture of lower-abundance proteins. The process was highly reproducible between the different runs, leading to four major populations. P1 population was first collected in the flow through, followed by the elution of the three other ones in a NaCl gradient. The protein yield calculated from the $A_{260\,nm}$ and $A_{280\,nm}$ registrations was ∼73% for each run. According to the $A_{260\,nm}/A_{280\,nm}$ ratios, the first three populations were constituted mainly of proteins, and the fourth one contained 10% residual DNA despite spermin precipitation after cell lysis. The protein content of the cell extract and the four populations from ion-exchange chromatography were analysed by proteomic analysis prior to the affinity step. In order to check for the most abundant proteins of each population, we ran 2D-PAGE gels (Fig. 1 and the related Table 1) and identified the main spots of proteins, using tandem mass spectrometry sequencing (LC–ESI-MS/MS). One hundred and seventy three spots were analyzed, leading to the identification of 118 different proteins. The number and colour intensity of the spots gave us a visual estimate of each amount of protein. The chromatographic process was highly reproducible and a slight overlap between the protein populations of two consecutive fractions was observed on the chromatograms. The four populations were then extensively dialyzed in the binding buffer (pH 7.4) before IMAC enrichment.

3.2. Capture and identification of UO_2-IMAC-isolated proteins

The previous P1–P4 populations were subjected to UO_2-IMAC in a batch system with uranyl-loaded Duolite C467^{TM} beads. Simultaneous control runs were always performed with a free uranyl support. The processes were reproduced twice at least for each sample. Protein capture was monitored by UV–vis absorption in the supernatants. A high salt concentration in the binding buffer (0.5 M NaCl) and surfactant supplementation (0.05% Brij) ensured very low non-specific binding such as ion-exchange phenomena with the immobilized cations and/or the remaining aminophosphonate groups of the Duolite C467^{TM} and hydrophobic interactions. Weak interactions were prevented by adding 1 mM of $NaHCO_3$, a chelating agent for uranyl ions acting as a strong competitor with proteins in submicromolar concentration ranges. Furthermore, $NaHCO_3$ is naturally present in the intracellular fluids. After several washes (140 column volumes) and overnight dialysis against the binding buffer, any non-specifically bound proteins were removed. We only considered as proteins of interest those which were eluted by 0.2 M sodium carbonate in two different runs.

The contents of the eluted F1–F4 fractions, directly corresponding to the P1–P4 populations of the ion-exchange chromatography, were analysed by nano-LC–ESI-MS/MS. Each nano-LC run was also performed in duplicate and preceded by one or two blank runs to ensure the lack of cross-contamination. As previously observed [15], the capture conditions and washing steps were efficient enough to prevent the proteins from non-specific or weak binding of charged groups (i.e. phospho- groups, acidic amino acids...) onto the IMAC phase, since we never detected any protein in the fractions eluted from the different control runs. The process favored strong interactions such as coordination. The proteins eluted from the uranyl-loaded beads were classified using the Mascot score, which is partly linked to the number of sequenced peptides and to protein abundance. We took into account two different sequenced peptides for each proteins and a statistical score above identity threshold. Under these stringent conditions we identified 77 proteins in the F1–F4 fractions, 64 of which were different (Table 2). This number is within the range of captured proteins from different IMAC processes [26,28,38].

The IMAC process was highly reproducible and the three following observations confirmed its efficiency and selectivity. First, protein recovery was not directly related to the protein amount in each fraction. In spite of the highly populated 2D-PAGE of the P2 population from the ion-exchange step, few proteins were captured and eluted in the corresponding F2 fraction. Second, the slight protein overlap observed between two ion-exchange populations induces the capture of the same proteins in two different IMAC runs. For instance, the protein ACTB was mainly found in P3 but

Table 2
Identification of UO_2-IMAC proteins.

Fraction	Protein name	ID	Gene name	Swiss Prot accession number	Mascot score
F1	Alpha-enolase	ENOA	ENO1	P06733	997
	AnnexinA2	ANXA2	ANXA2	P07355	971
	Transketolase	TKT	TKT	P29401	532
	Cofilin-1	COF1	CFL1	P23528	514
	10 kDa heat shock protein	CH10	HSPE1	P61604	499
	Peptidyl-prolyl cis-trans isomerase B	PPIB	PPIB	P23284	476
	Annexin A1	ANXA1	ANXA1	P04083	462
	Fructose-bisphosphate aldolase A	ALDOA	ALDOA	P04075	461
	Peroxiredoxin 1	PRDX1	PRDX1	Q06830	423
	Collagen-binding protein 2	SERPH	SERPINH1	P50454	360
	Peptidyl-prolyl cis–trans isomerase A	PPIA	PPIA	P62937	320
	Phosphoglycerate kinase 1	PGK1	PGK1	P00558	310
	Nucleoside diphosphate kinase B	NDKB	NME2	P22392	301
	DNA-(apurinic or apyrimidinic site) lyase	APEX	APEX1	P27695	257
	ARMET protein	ARMET	ARMET	P55145	253
	Transgelin-2	TAGL2	TAGLN2	P37802	213
	Destrin	DEST	DSTN	P60981	209
	Elongation factor 1-alpha 2	EF1A2	EEF1A2	Q05639	207
	Elongation factor 1-alpha 1	EF1A1	EEF1A1	P68104	190
	L-lactate dehydrogenase A chain	LDHA	LDHA	P00338	167
	Poly [ADP-ribose] polymerase 1	PARP1	PARP1	P09874	158
	Glyceraldehyde-3-phosphate dehydrogenase	G3P	GAPDH	P04406	142
	Peroxiredoxin 5	PRDX5	PRDX5	P30044	141
	Calgizzarin	S10A4B	S100A11	P31949	126
	Endothelial differentiation-related factor 1	EDF1	EDF1	O60869	98
	Adenylate kinase isoenzyme 1	KAD1	AK1	P00568	81
	Deoxycytidylate deaminase	DCTD	DCTD	P32321	71
F2	Moesin	MOES	MSN	P26038	311
	Protein disulfide-isomerase A3	PDIA3	PDIA3	P30101	273
	Annexin A5	ANXA5	ANXA5	P08758	229
	Ezrin	EZRI	VIL2	P15311	284
	Peroxiredoxin 1	PRDX1	PRDX1	Q06830	125
	Nucleoside diphosphate kinase B	NDKB	NME2	P22392	108
	Aldose reductase	ALDR	AKR1B1	P15121	189
	L-lactate dehydrogenase B chain	LDHB	LDHB	P07195	85
	Proteasome activator complex subunit 1	PSME	PSME1	Q06323	131
	Cofilin-1	COF1	CFL1	P23528	74
	Heterogeneous nuclear ribonucleoproteins A2/B1	ROA2	HNRNPA2B1	P22626	90
	Stathmin	STMN1	STMN1	P16949	67
	Annexin A3	ANXA3	ANXA3	P12429	94
	Ubiquitin carboxyl-terminal hydrolase isozyme L1	UCHL1	UCHL1	P09936	96
	L-lactate dehydrogenase A chain	LDHA	LDHA	P00338	98
F3	Protein disulfide-isomerase A4	PDIA4	PDIA4	P13667	840
	Heat shock protein HSP 90-alpha	HSP90A	HSP90AA1	P07900	619
	Actin B	ACTB	ACTB	P60709	423
	Protein disulfide-isomerase	PDIA1	P4HB	P07237	412
	Glucosidase II beta subunit	GLU2B	PRKCSH	P14314	353
	14-3-3 protein zeta/delta	1433Z	YWHAZ	P63104	323
	Actin, alpha cardiac	ACTC	ACTC1	P68032	312
	78 kDa glucose-regulated protein	GRP78	HSPA5	P11021	307
	Calreticulin	CALR	CALR	P27797	208
	14-3-3 protein epsilon	1433E	YWHAE	P62258	185
	Creatine kinase B-type	KCRB	CKB	P12277	183
	Peroxiredoxin-1	PRDX1	PRDX1	Q06830	162
	14-3-3 protein beta/alpha	1433B	YWHAB	P31946	126
	14-3-3 protein theta	1433T	YWHAQ	P27348	123
	ERO1-like protein alpha	ERO1A	ERO1L	Q96HE7	123
	14-3-3 protein theta	1433T	YWHAQ	P27348	117
	Protein disulfide-isomerase A6	PDIA6	PDIA6	Q15084	116
	Hepatoma-derived growth factor	HDGF	HDGF	P51858	111
	Protein disulfide-isomerase A3	PDIA3	PDIA3	P30101	110
	Ubiquitin carboxyl-terminal hydrolase	UCHL1	UCHL1	P09936	80
	Actin, aortic smooth muscle	ACTA	ACTA2	P62736	234
	RNA-binding protein 8A	RMB8A	RBM8A	Q9Y5S9	133
	Neutral alpha-glucosidase AB	GANAB	GANAB	Q14697	123
	Elongation factor 1-beta	EF1B	EEF1B2	P24534	88
	Thioredoxin-dependent peroxide reductase	PRDX3	PRDX3	P30048	85
	Calmodulin	CALM	CALM2	P62158	84
	GTP-binding nuclear protein	RAN	RAN	P62826	77
F4	Calreticulin	CALR	CALR	P27797	170
	Actin B	ACTB	ACTB	P60709	165
	Acidic leucine-rich nuclear phosphoprotein 32 A	AN32A	ANP32A	P39687	165

Table 2 (*Continued*)

Fraction	Protein name	ID	Gene name	Swiss Prot accession number	Mascot score
	Acidic leucine-rich nuclear phosphoprotein 32 B	AN32B	ANP32B	Q92688	165
	SET protein	SET	SET	Q01105	134
	Protein disulfide-isomerase	PDIA1	P4HB	P07237	129
	Glucosidase II beta subunit	GLU2B	PRKCSH	P14314	128
	78 kDa glucose-regulated protein	GRP78	HSPA5	P11021	108
	14-3-3 protein zeta/delta	1433Z	YWHAZ	P63104	84

The four populations (P1–P4) obtained by ion-exchange chromatography were brought into contact with the IMAC phase leading to the four corresponding fractions (F1–F4). The proteins were identified by Nano-LC–ESI-MS/MS. For each fraction we ran two biological replicates and for each two technical replicates (Nano-LC–ESI-MS/MS runs). We validated the identified proteins with two correctly fragmented peptides (i.e. with a Mascot score above identity for each peptide). Proteins in bold characters were identified on the 2D-PAGE gels of the P1–P4 populations (supplementary data).

also in P4 populations. It was consequently isolated in the F3 and F4 fractions. Third, the proteins identified were not always the most abundant proteins in the HK-2 cell extract: the minor protein PRDX1 was never detected among the main spots in the first three 2D-PAGE gels corresponding to the P1–P3 populations from ion-exchange, but was identified in the mass spectra analysis of fractions F1–F3. Twenty-three proteins isolated from UO2-IMAC were previously identified among the 118 proteins of ion-exchange populations. So the captured proteins identified in the IMAC process were not just abundant proteins present in the P1–P4 populations.

For each fraction, we checked for proteins which might have been co-eluted because of pre-existing protein–protein interaction. We used the IPA 6.0 software (as described in Section 2) and found few possible direct interactions in F1, F2 and F4. In F1 fraction ANXA1, ANXA2 and EF1A1 might be co-eluted; this is also the case in F2 for MOES and EZRI, LDHA and LDHB, and in F4 for SET and AN32A. These protein–protein heteromers could be slightly more numerous in the F3 fraction (Supplementary data, figure* S1). So, despite the high ionic strength in the binding buffer, the hypothesis of direct protein–protein interaction leading to co-elution cannot be totally discarded, but was certainly not a dominating event.

One can wonder whether the results would have been identical using any another metal, due for example to an alternation of negatively and positively charged groups (phosphonic groups and metallic ions) on the support surface. The electrostatic/ionic and hydrophobic interactions might have a relative contribution in the binding, even though the chromatographic conditions weakened them. So to further investigate the selectivity/specificity of the protein binding we tested the incidence of another hard Lewis cation by loading the beads with Fe^{3+} ions. These ions are also known to bind strongly to phosphonate groups [39]. So we did not evaluate carefully the properties of this phase, but only checked that ferric ions were not desorbed in a blank run. Because the protein content of P2 displayed various MW and PI, we decided to contact this population with the iron-loaded beads. The sample conditioning and the protein capture were strictly identical for both supports. For elution, instead of carbonate in the UO_2-IMAC, we used citrate as competitor in the Fe-IMAC because it is a better chelating agent for ferric ions. Table 3 presents the comparative results obtained with both metals. They revealed divergent selectivity, with 13 proteins captured only on the Fe^{3+} loaded phase and six proteins only by the $UO_2{}^{2+}$ loaded phase. One third (9/28) was common to both supports, adding the two proteins ANXA2 and GRP78 captured by the Fe-IMAC and also identified in the F1 and F3 fractions respectively from UO_2-IMAC (Table 2).

Similar population overlapping between copper and zinc binding proteins are reported [36,38,40] and explained by relative affinities of some proteins with respect to these two hard cations. However, two-thirds non-common proteins assess the process selectivity.

Table 3
Comparison of proteins eluted from UO_2-IMAC or Fe-IMAC.

Protein name	ID	Swiss Prot accession number
Proteins bound on both columns		
Aldose reductase	ALDR	P15121
Annexin A3	ANXA3	P12429
AnnexinA5	ANXA5	P08758
Ezrin	EZRI	P15311
L-lactate dehydrogenase A chain	LDHA	P00338
Moesin	MOES	P26038
Protein disulfide-isomerase A3 precursor	PDIA3	P30101
Peroxiredoxin 1	PRDX1	Q06830
Heterogeneous nuclear ribonucleoproteins A2/B1	ROA2	P22626
Proteins bound on UO_2-IMAC		
L-lactate dehydrogenase B chain	LDHB	P07195
Ubiquitin carboxyl-terminal hydrolase	UCHL1	P09936
Stathmin	STMN1	P16949
Nucleoside diphosphate kinase B	NDKB	P22392
Cofilin-1	COF1	P23528
Proteasome activator complex subunit 1	PSME1	Q06323
Proteins bound on Fe-IMAC		
Annexin A2	ANXA2	P07355
Proactivator polypeptide	SAP	P07602
Glutathione S-transferase P	GSTP1	P09211
Annexin A4	ANXA4	P09525
Heterogeneous nuclear ribonucleoprotein A1	ROA1	P09651
Thioredoxin	THIO	P10599
78 kDa glucose-regulated protein precursor	GRP78	P11021
Vinculin	VINC	P18206
Phosphoglycerate mutase 1	PGAM1	P18669
Peroxiredoxin 6	PRDX6	P30041
Transaldolase	TALDO	P37837
Malate dehydrogenase	MDHC	P40925
Rab GDP dissociation inhibitor beta	GDIB	P50395

The P2 population was applied to Fe-IMAC and the captured proteins were compared to the protein content of F2. Identification was performed by using Nano-LC–ESI-MS/MS. The same stringent identification procedure (see Table 1 was applied to validate the proteins.

Table 4
Analysis of IMAC captured proteins according to ligand-based properties.

Swiss Prot accession number	ID	Score	Maximum sequence coverage	Cation	Phosphorylation	Biomolecule-phospho-
P30101	PDIA3	−1050	48%	Ca^{2+}, Zn^{2+}	No	
P62158	CALM	−893	99%	Ca^{2+}	Multiple	
Q01105	SET	−854	69%		Multiple	
P07355	ANXA2	−787	100%	2 Ca^{2+}	Multiple	Phospholipids
P15311	EZRI	−763	50%		Multiple	Phosphatidyl inositol
P62826	RAN	−748	100%		Single	GTP binding
P00568	KAD1	−741	99%	Zn^{2+}	No	ATP
P04083	ANXA1	−703	90%	2–4 Ca^{2+}	Multiple	Phospholipids
P62937	PPIA	−690	99%		Multiple	
P27695	APEX1	−686	100%	Mg^{2+}, Mn^{2+}	Single	DNA
P07900	HSP90A	−679	32%		Multiple	ATPase
P08758	ANXA5	−657	100%	Ca^{2+}	No	Phospholipids
P24534	EF1B	−654	40%		Multiple	
Q9Y5S9	RBM8A	−649	62%		Multiple	RNA
P26038	MOES	−631	60%		Multiple	
P07195	LDHB	−618	100%		Single	
P12429	ANXA3	−611	100%	Ca^{2+}	No	
P23284	PPIB	−597	85%		No	
P04075	ALDOA	−557	100%		Multiple	
P51858	HDGF	−514	41%		Multiple	DNA
P15121	ALDR	−508	100%		Multiple	NADP
P07237	PDIA1	−500	23%		No	
P27348	1433T	−488	95%		No	Phosphoserine, phosphothreonine
Q15084	PDIA6	−475	27%		Single	
Q06830	PRDX1	−473	99%		Multiple	
P39687	AN32A	−471	59%		Single	
P63104	1433Z	−454	100%		Multiple	Phosphorylated-MLF1
P09874	PARP1	−439	34%	Zn^{2+}	Single	Poly ADP ribose
P22626	ROA2	−435	29%		Multiple	mRNA processing
P37802	TAGL2	−432	71%		Multiple	
P09936	UCHL1	−419	100%		Multiple	
P27797	CALR	−411	2%	Ca^{2+}	No	
P31946	1433B	−408	97%		Single	Phosphoserine
P00338	LDHA	−405	100%		Single	NAD
P23528	COF1	−398	99%		Multiple	Phosphoinositol
P30044	PRDX5	−394	75%		No	
Q06323	PSME	−393	80%		No	
P04406	G3P	−346	100%	Zn^{2+}, Cu^{2+}	Multiple	NAD
O60869	EDF1	−208	52%		No	
P62258	1433^{E}	−208	91%		Single	
P00558	PGK1			Mg^{2+}	Multiple	ATP, phosphoglycerate
P06733	ENOA			Mg^{2+}, Zn^{2+}	Multiple	Phosphoglycerate
P11021	GRP78				Multiple	
P12277	KCRB				Multiple	ATP
P13667	PDIA4				No	
P14314	GLU2B				Multiple	
P16949	STMN1				Multiple	
P29401	TKT			Ca^{2+}	Multiple	Sedoheptulose 7P
P30048	PRDX3				No	
P31949	S10A4B		17%	2 Ca^{2+}	Single	
P32321	DCTD			Zn^{2+}	Single	dCMP
P50454	SERPH				No	
P55145	ARMET				Single	
P60709	ACTB			Mg^{2+}	Multiple	Mg ATP
P60981	DEST				Single	
P61604	CH10				No	
P62736	ACTA				No	
P68032	ACTC				No	
P68104	EF1A1		95%	Mg^{2+}	Single	GTP glycerophosphoryl ethanolamine
Q05639	EF1A2				Single	GTP glycerophosphoryl ethanolamine
Q14697	GANAB				No	
Q92688	AN32B				Single	
Q96HE7	ERO1A				No	
P22392	NDKB		99%	Mg^{2+}	No	ATP, DNA

Proteins were identified through their Swiss Prot accession number and ID, and categorized according to the following characteristics: “score” refered to uranyl–protein complex energy and was calculated with the metal-docking tool when structural data were available. A score value less than −500 is significant to predict an uranyl binding site; “maximum sequence coverage” was computed from Swiss Prot and PDB sequence lengths; “cation”, “phosphorylation”, and “biomolecule-phospho-” interaction data were from the Swiss Prot database; the information was validated by a thorough bibliographic research. Underlined Swiss Prot accession numbers correspond to proteins with acidic motifs.

3.3. Protein analysis: functional properties

A functional analysis of our data set of 64 non-redundant captured proteins was performed with IPA 6.0 software. Representative categories of biological functions in which the proteins were dispatched are given in (Supplementary data Table S1) (p-value < 0.002). Although if we have to keep in mind that transcriptomic results are not directly correlated to proteomic ones,

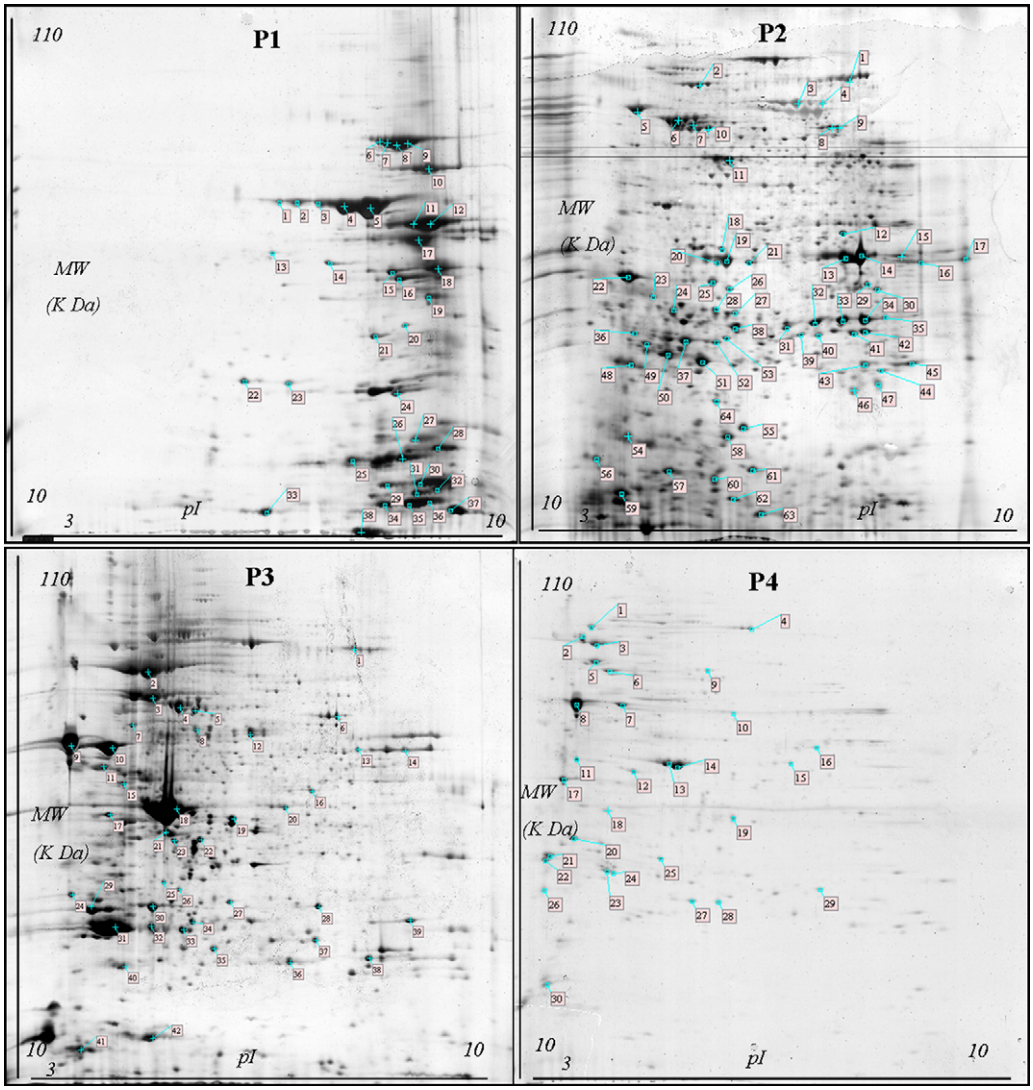

Fig. 2. Silver stained 2D-PAGE of the four pre-fractionated populations (P1-P4) by ion-exchange. The identified proteins were labelled on the figure (see Table 1).

some proteins from the list attracted our attention, i.e. LDHA, ENOA, 1433T, PPIA, RAN, STMN1, ACTB, EF1A1, CALM, HSP90A, because they also belong to proteins whose gene expression changed after exposure of cultured HEK293 (human embryonic kidney cells) to uranyl [17].

So, as previously observed by similar studies dedicated to other varied metals [21,23], the 64 identified proteins displayed a wide range of cellular functions. We therefore needed to analyze these results from a different angle. Affinity chromatography cannot be a "stand-alone" one-dimensional identification process in proteomics [41]. Complementary approaches are always necessary to analyze the properties of the captured proteins. For example, the presence of $C(X)_nC$ ($n=2$ or 4) or $H(X)_mH$ ($m=0$–5) motifs in the proteins eluted from immobilized copper affinity chromatography reinforces the assumption of copper-affine sites [21]. But descriptions of uranyl sites in proteins are very scarce, and we examined the properties which could explain a binding onto the UO_2-IMAC Fig. 2.

3.4. Protein analysis: physicochemical properties

We examined four ligand-based properties which might explain the IMAC capture of the proteins: (a) the existence of surface-exposed residues with compatible geometry for uranyl chelation in a binding site; (b) an affinity for hard Lewis cations; (c) the presence of phosphorylated groups, considering the affinity of uranyl for phosphorous containing compounds [11,12,42–46]; (d) the ability to establish interaction with a phospho-containing entity, (designated as a "biomolecule-phospho-"), as possible mimicry of binding to uranyl phosphonate groups in the IMAC process. To summarize this analysis, the different possible bonds between the proteins and the uranyl cation in varied environments are illustrated in Fig. 3. The extensive list of proteins categorized according to these criteria is given in Table 4.

We first applied the metal-docking tool developed in the laboratory to determine the proteins presenting surface exposed-residues with a well adapted geometry to allow the binding of uranyl. This analysis could be set up only with a subset of 43 among 64 proteins for which a partial or total structural description was available in the Protein DataBank ("coverage sequence" column). They were first classified according to decreasing theoretical scores, for which a value of less than −500 is statistically significant to predict an uranyl binding site. Thus, such a site was expected for 22 among these 43 proteins (51%). But we cannot exclude the fact that low score values (above −500) obtained with low sequence coverage might be false negatives, as CALR for which a structural description refers only to 2% of the protein. There was no available structure for the 21 remaining proteins.

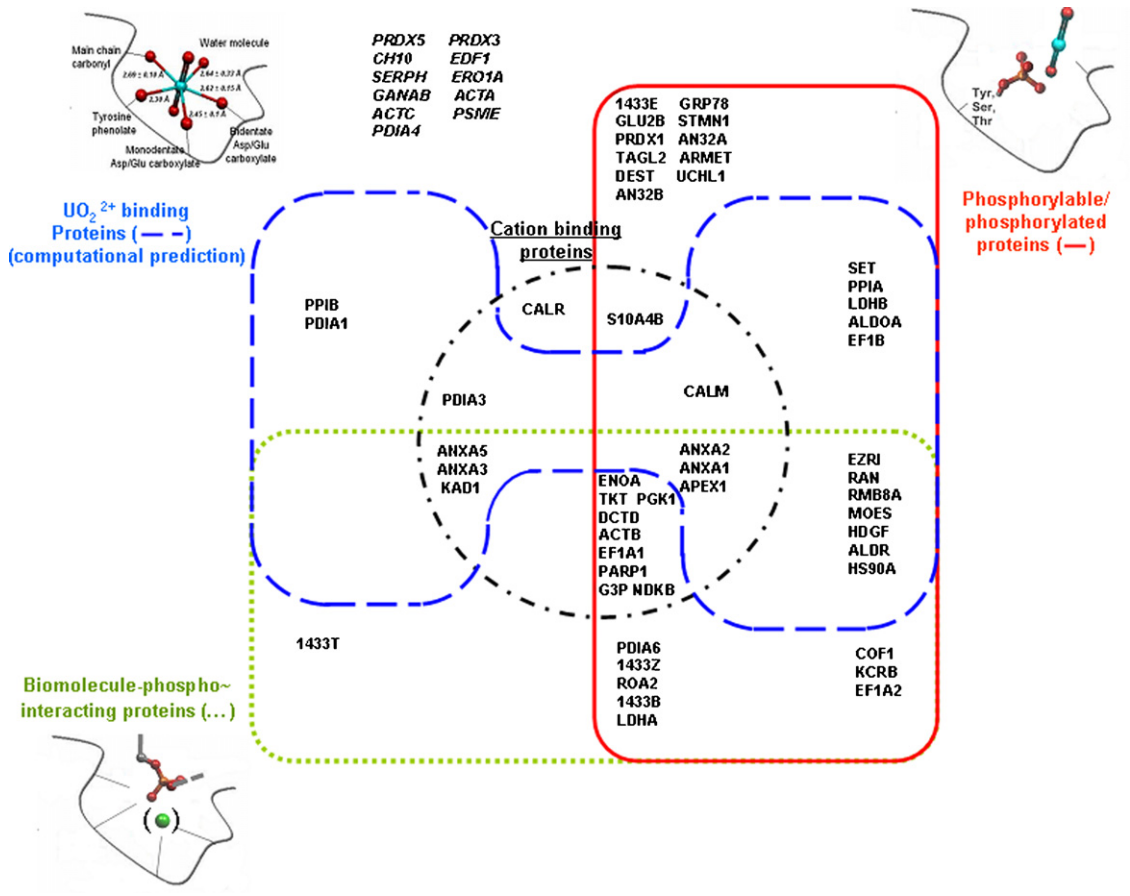

Fig. 3. Schema of the protein distribution according to ligand-based properties (see Table 4). (a) Predicted UO_2^{2+} binding site (dash trace), (b) hard-cation binding properties (hyphen trace), (c) potential phosphorylations (continuous trace) and (d) ability to interact with biomolecules carrying phospho-groups or cations (dotted trace) were merged into the diagram. Schematics on the sides illustrate the possible modalities of binding per category.

The whole protein data set was analyzed according to the three other criteria. Of the 64 listed proteins, 19 (~30%) are also described as hard Lewis cation (Ca^{2+}, Zn^{2+}, Mn^{2+} or Mg^{2+}) binding proteins, as for example ANXA5, CALR, ENO1, GRP78, PDI and CALM. The proteins predicted to have phosphorylation sites were also largely represented (44/64 i.e. ~69% of the protein data set), which is significantly and statistically higher than in the global proteome (about one-third) [47,48]. Of those, 28 among 64 proteins were potentially poly-phosphorylated. Strikingly, 44% of the proteins could present phosphotyrosine groups, which is a much higher level than in the global phospho-proteome (~1%) [47,48]. Nevertheless, phosphorylations are transient and reversible phenomena. Further studies are needed to evaluate if the binding of these proteins is directly correlated or not to their phosphate content. In their work dedicated to Fe-IDA Porath and Andersson [36] demonstrated the specificity of phosphoproteins to bind to Fe^{3+}, whereas unphosphorylated albumin did not display any affinity for this support. Here, part of proteins probably obeyed similar mechanisms of binding either on Fe-IMAC or UO_2-IMAC, in particular resulting in the overlapping between the enriched populations. But potentially unphosphorylated proteins are also captured in the UO_2-IMAC system.

Then, according to the fourth criterion, we observed that 45% of the proteins were known to bind to various biomolecules carrying phospho-ligands (such as phospho-serine or threonine). On one hand, the use of a high ionic strength in the process prevented the ionic interactions between the proteins and the uranyl-loaded phase. On the other hand, interaction with phosphonate groups cannot be reasonably suspected, since no binding occurred between the metal-free IMAC phase and the proteins, providing evidence that UO_2^{2+} is essential in the binding process. The presence of carbonate also limited the weak interactions. Thus, only a strong coordination binding between the metal and ligands can explain this type of recognition. However, the presence of acidic (asp-glu or glu) rich regions inside the proteins was checked, as they might be potential unspecific binding sites for hard cations. Only few proteins (5/64) presented these properties, demonstrating that the IMAC process did not specifically enhance the capture of proteins having acidic clusters. Lastly, of the 64 proteins, 11 proteins are excluded from the diagram. The main reason is that the current protein annotation and the lack of structure information cannot lead to their categorization.

4. Conclusion

Until now, there is no efficient and straightforward technique to discriminate between potential uranyl targets and others. Chromatographic strategies based on molecular recognition provide useful tools for selective capture of proteins. To our knowledge, this proteomic strategy based on the specifically designed and validated uranyl affinity chromatography [15] presents the first results for the enrichment of UO_2^{2+}-interacting proteins, at physiological pH and starting from human cell extracts. The ionic strength conditions applied in the chromatography along with the supplementation of surfactant and competitor avoided the weak bindings thus favouring stronger interactions such as coordination. The pH was within physiological range. The process led to the selective capture and identification of 64 proteins from thousands in such a cell extract. These proteins were not all the inevitably high abundance proteins.

To check the specificity of the UO_2-IMAC, we set up experiments either with Fe^{3+} or $UO_2{}^{2+}$ loaded phases. From one of the most variously populated of the pre-fractionated protein samples, part of eluted populations was significantly different demonstrating a cation selectivity. An overlapping in the protein content of the captured populations was also observed. The ability for the proteins to bind to different hard cations does not exclude their relative potential toxic effect, according to their affinity range. And without a tightly regulated homeostasis, beneficial metals such as Fe^{3+} also have noxious effects at high level.

The analysis of protein collections resulting from an IMAC process remains a challenge because the captured proteins are often numerous and also play parts in multiple pathways. Furthermore, the lack of knowledge concerning the binding-sites of some exogenous metals like uranyl is a handicap for more rationalized approaches. Here, the use of a metal-docking tool, along with a screening based on known ligand properties of $UO_2{}^{2+}$ ion, allowed us to categorize the captured proteins highlighting a possible relative importance of the phosphorylations and/or phospho-group binding properties. Since the stoichiometry of phosphorylations is generally low and heterogeneous at any given time, the phosphorylations of these proteins remain now to be checked. These results will give information on the capacity of this UO_2-IMAC to bind phosphoproteins, but also would reinforce studies on the toxicological impact of uranyl cations via phosphorylations.

Finally, this work constitutes one approach to identify uranyl targets, and although it is difficult to determine an affinity range from IMAC processes, merging the categorization criteria enables us to focus on some proteins displaying interesting characteristics for further studies.

Acknowledgements

We gratefully thank Dr. Didier Cavadore (Laboratoire d'Analyses Biologiques et Médicales, CEA Marcoule) for ICP-MS measurements, Florence Hely-Joly, Philippe Guérin and Ludovic Mikalef for technical assistance.

This work was partly supported by the CEA Program "Toxicologie Nucleaire Environnementale".

Appendix A. Supplementary data

Supplementary data associated with this article can be found, in the online version, at doi:10.1016/j.chroma.2009.05.023.

References

[1] R.W. Leggett, T.C. Pellmar, J. Environ. Radioact. 64 (2003) 205.
[2] V. Lemercier, X. Millot, E. Ansoborlo, F. Menetrier, A. Flury-Herard, C. Rousselle, J.M. Scherrmann, Radiat. Prot. Dosim. 105 (2003) 243.
[3] E. Arnault, M. Doussau, A. Pesty, B. Gouget, A. Van der Meeren, P. Fouchet, B. Lefevre, Toxicology 247 (2008) 80.
[4] R.W. Leggett, Health Phys. 57 (1989) 365.
[5] D.M. Taylor, S.K. Taylor, Rev. Environ. Health 12 (1997) 147.
[6] M. Carriere, L. Avoscan, R. Collins, F. Carrot, H. Khodja, E. Ansoborlo, B. Gouget, Chem. Res. Toxicol. 17 (2004) 446.
[7] M. Carriere, C. Thiebault, S. Milgram, L. Avoscan, O. Proux, B. Gouget, Chem. Res. Toxicol. 19 (2006) 1637.
[8] P. Kurttio, A. Harmoinen, H. Saha, L. Salonen, Z. Karpas, H. Komulainen, A. Auvinen, Am. J. Kidney Dis. 47 (2006) 972.
[9] C. De Stefano, A. Gianguzza, A. Pettignano, S. Sammartano, Biophys. Chem. 117 (2005) 147.
[10] K.E. Rich, R.T. Agarwal, I. Feldman, J. Am. Chem. Soc. 92 (1970) 6818.
[11] R.P. Agarwal, I. Feldman, J. Am. Chem. Soc. 90 (1968) 6635.
[12] W.J. Hartsock, J.D. Cohen, D.J. Segal, Chem. Res. Toxicol. 20 (2007) 784.
[13] C. Vidaud, A. Dedieu, C. Basset, S. Plantevin, I. Dany, O. Pible, E. Quemeneur, Chem. Res. Toxicol. 18 (2005) 946.
[14] C. Vidaud, S. Gourion-Arsiquaud, F. Rollin-Genetet, C. Torne-Celer, S. Plantevin, O. Pible, C. Berthomieu, E. Quemeneur, Biochemistry 46 (2007) 2215.
[15] C. Basset, A. Dedieu, P. Guerin, E. Quemeneur, D. Meyer, C. Vidaud, J. Chromatogr. A 1185 (2008) 233.
[16] H.J. MacCordick, F. Taghva, J.P. Meyer, D. Gelus, J. Radioanal. Nucl. Chem. 223 (1997) 187.
[17] O. Prat, F. Berenguer, V. Malard, E. Tavan, N. Sage, G. Steinmetz, E. Quemeneur, Proteomics 5 (2005) 297.
[18] O. Prat, F. Berenguer, V. Malard, S. Ruat, G. Steinmetz, E. Tavan, E. Quemeneur, Toxicol. Lett. 164 (2006) S297.
[19] O. Prat, F. Berenguer, V. Malard, E. Tavan, G. Steinmetz, E. Quemeneur, Toxicol. Appl. Pharm. 197 (2004) 266.
[20] O. Pible, P. Guilbaud, J.L. Pellequer, C. Vidaud, E. Quemeneur, Biochimie (2006) 1631.
[21] S.D. Smith, Y.M. She, E.A. Roberts, B. Sarkar, J. Proteome Res. 3 (2004) 834.
[22] H. Roelofsen, R. Balgobind, R.J. Vonk, J. Cell. Biochem. 93 (2004) 732.
[23] R. Ge, X. Sun, Q. Gu, R.M. Watt, J.A. Tanner, B.C. Wong, H.H. Xia, J.D. Huang, Q.Y. He, H. Sun, J. Biol. Inorg. Chem. 12 (2007) 831.
[24] D.S. Hage, Clin. Chem. 45 (1999) 593.
[25] S.B. Ficarro, M.L. McCleland, P.T. Stukenberg, D.J. Burke, M.M. Ross, J. Shabanowitz, D.F. Hunt, F.M. White, Nat. Biotechnol. 20 (2002) 301.
[26] A. Dubrovska, S. Souchelnytskyi, Proteomics 5 (2005) 4678.
[27] M. Machida, H. Kosako, K. Shirakabe, M. Kobayashi, M. Ushiyama, J. Inagawa, J. Hirano, T. Nakano, Y. Bando, E. Nishida, S. Hattori, FEBS J. 274 (2007) 1576.
[28] I.C. Guerrera, J. Predic-Atkinson, O. Kleiner, V. Soskic, J. Godovac-Zimmermann, J. Proteome Res. 4 (2005) 1545.
[29] M.O. Collins, L. Yu, M.P. Coba, H. Husi, I. Campuzano, W.P. Blackstock, J.S. Choudhary, S.G. Grant, J. Biol. Chem. 280 (2005) 5972.
[30] T.O. Metz, W.J. Qian, J.M. Jacobs, M.A. Gritsenko, R.J. Moore, A.D. Polpitiya, M.E. Monroe, D.G. Camp 2nd, P.W. Mueller, R.D. Smith, J. Proteome Res. 7 (2008) 698.
[31] I. Feuerstein, M. Rainer, K. Bernardo, G. Stecher, C.W. Huck, K. Kofler, A. Pelzer, W. Horninger, H. Klocker, G. Bartsch, G.K. Bonn, J. Proteome Res. 4 (2005) 2320.
[32] J. Hardouin, R. Joubert-Caron, M. Caron, J. Sep. Sci. 30 (2007) 1482.
[33] Y.J. Zhao, E. Sulkowski, J. Porath, Eur. J. Biochem. 202 (1991) 1115.
[34] E.S. Hemdan, Y.J. Zhao, E. Sulkowski, J. Porath, Proc. Natl. Acad. Sci. U.S.A. 86 (1989) 1811.
[35] L.P. Pathange, D.R. Bevan, T.J. Larson, C. Zhang, Anal. Chem. 78 (2006) 4443.
[36] L. Andersson, J. Porath, Anal. Biochem. 154 (1986) 250.
[37] M.J. Ryan, G. Johnson, J. Kirk, S.M. Fuerstenberg, R.A. Zager, B. Torok-Storb, Kidney Int. 45 (1994) 48.
[38] Y.M. She, S. Narindrasorasak, S. Yang, N. Spitale, E.A. Roberts, B. Sarkar, Mol. Cell. Proteomics 2 (2003) 1306.
[39] R. Burgada, T. Bailly, M. Lecouvey, C.R. Chimie 7 (2004) 35.
[40] C.C. Kung, W.N. Huang, Y.C. Huang, K.C. Yeh, Proteomics 6 (2006) 2746.
[41] A.C. Roque, C.R. Lowe, Biotechnol. Adv. 24 (2006) 17.
[42] S.D. Alexandratos, X. Zhu, React. Funct. Polym. 67 (2007) 375.
[43] M. Sawicki, D. Lecercle, G. Grillon, B. Le Gall, A.L. Serandour, J.L. Poncy, T. Bailly, R. Burgada, M. Lecouvey, V. Challeix, A. Leydier, S. Pellet-Rostaing, E. Ansoborlo, F. Taran, Eur. J. Med. Chem. 43 (2008) 2768.
[44] M. Sawicki, J.M. Siaugue, C. Jacopin, C. Moulin, T. Bailly, R. Burgada, S. Meunier, P. Baret, J.L. Pierre, F. Taran, Chemistry 11 (2005) 3689.
[45] G.J. Vazquez, C.J. Dodge, A.J. Francis, Chemosphere 70 (2007) 263.
[46] A. Koban, G. Bernhard, J. Inorg. Biochem. 101 (2007) 750.
[47] M. Mann, S.E. Ong, M. Gronborg, H. Steen, O.N. Jensen, A. Pandey, Trends Biotechnol. 20 (2002) 261.
[48] J.C. Venter, M.D. Adams, E.W. Myers, P.W. Li, R.J. Mural, G.G. Sutton, H.O. Smith, M. Yandell, C.A. Evans, R.A. Holt, J.D. Gocayne, P. Amanatides, R.M. Ballew, D.H. Huson, J.R. Wortman, Q. Zhang, C.D. Kodira, X.H. Zheng, L. Chen, M. Skupski, G. Subramanian, P.D. Thomas, J. Zhang, G.L. Gabor Miklos, C. Nelson, S. Broder, A.G. Clark, J. Nadeau, V.A. McKusick, N. Zinder, A.J. Levine, R.J. Roberts, M. Simon, C. Slayman, M. Hunkapiller, R. Bolanos, A. Delcher, I. Dew, D. Fasulo, M. Flanigan, L. Florea, A. Halpern, S. Hannenhalli, S. Kravitz, S. Levy, C. Mobarry, K. Reinert, K. Remington, J. Abu-Threideh, E. Beasley, K. Biddick, V. Bonazzi, R. Brandon, M. Cargill, I. Chandramouliswaran, R. Charlab, K. Chaturvedi, Z. Deng, V. Di Francesco, P. Dunn, K. Eilbeck, C. Evangelista, A.E. Gabrielian, W. Gan, W. Ge, F. Gong, Z. Gu, P. Guan, T.J. Heiman, M.E. Higgins, R.R. Ji, Z. Ke, K.A. Ketchum, Z. Lai, Y. Lei, Z. Li, J. Li, Y. Liang, X. Lin, F. Lu, G.V. Merkulov, N. Milshina, H.M. Moore, A.K. Naik, V.A. Narayan, B. Neelam, D. Nusskern, D.B. Rusch, S. Salzberg, W. Shao, B. Shue, J. Sun, Z. Wang, A. Wang, X. Wang, J. Wang, M. Wei, R. Wides, C. Xiao, C. Yan, et al., Science 291 (2001) 1304.